

## Steps toward interstellar silicate mineralogy

### VI. Dependence of crystalline olivine IR spectra on iron content and particle shape

D. Fabian<sup>1</sup>, T. Henning<sup>1</sup>, C. Jäger<sup>1</sup>, H. Mutschke<sup>1</sup>, J. Dorschner<sup>1</sup>, and O. Wehrhan<sup>2</sup>

<sup>1</sup> Astrophysical Institute and University Observatory, University of Jena, Schillergässchen 3, 07745 Jena, Germany

<sup>2</sup> Institute for Optics and Quantumelectronics, University of Jena, Max-Wien-Platz 1, 07745 Jena, Germany

Received 1 February 2001 / Accepted 22 August 2001

**Abstract.** Crystalline olivines are an important component of silicate dust particles in space. ISO observations revealed the presence of crystalline silicates in comets, protoplanetary accretion disks, and outflows from evolved stars. For the interpretation of astronomical spectra, the relevant material data at a variety of temperatures and over a broad wavelength range, are urgently needed. In contrast to this need, optical properties of the astronomically interesting olivines are scarcely available at present. In order to close this gap, we studied the optical properties of three minerals of the olivine group by reflection spectroscopy on single crystals in the infrared spectral range. We measured the iron endmember (fayalite,  $\text{Fe}_2\text{SiO}_4$ ), an Mg-rich olivine ( $\text{Mg}_{1.9}\text{Fe}_{0.1}\text{SiO}_4$ ), and the magnesium endmember (forsterite,  $\text{Mg}_2\text{SiO}_4$ ) of the  $(\text{Mg}, \text{Fe})_2\text{SiO}_4$  series. For a direct comparison with astronomical observations, we present calculated mass absorption coefficients in the Rayleigh limit for different shapes and varying iron content of the dust particles. The laboratory data together with a set of ISO data for envelopes around evolved stars (Molster 2000) are used to constrain the properties of circumstellar silicates. We find that essentially all band positions are shifted to larger wavelengths with increasing iron content. The particle shape influences very significantly the strong bands such as the  $\text{B}_{1u}:\nu_3$  mode that appears as the “11.4  $\mu\text{m}$ ” band of forsterite, whereas e.g. the two FIR modes longward of 40  $\mu\text{m}$  remain practically unaffected by the particle shape but shift due to increasing iron content. The comparison with the band positions in ISO spectra points to the presence of olivine crystals strongly elongated along the crystallographic  $c$ -axis. In addition, we apply the calculated mass absorption coefficients to evaluate transmission measurements of particles embedded in a matrix – a technique which is frequently used in laboratory astrophysics. All data shown in this paper will be made available in digital form via the electronic database <http://www.astro.uni-jena.de>.

**Key words.** stars: circumstellar matter – stars: formation – stars: AGB and post-AGB – solar system: formation – methods: laboratory

#### 1. Introduction

The ISO mission revealed the presence of crystalline silicates around both evolved and young stars. Comparing the spectra to laboratory data suggests magnesium-rich olivine  $(\text{Mg}, \text{Fe})_2\text{SiO}_4$  and pyroxene  $(\text{Mg}, \text{Fe})\text{SiO}_3$  to be the major crystalline silicate components of most objects (see, e.g., Waters et al. 1996; Waelkens et al. 1996; Jäger et al. 1998; Waters et al. 1999; Molster 2000).

For radiative transfer computations needed to model spectra of circumstellar envelopes and disks, optical constants are always required. They serve as the basis for the calculation of the necessary absorption and scattering efficiencies for different size and shape distributions of the

dust particles. In order to broaden the database of optical constants, we present such data for three minerals of the olivine group with different iron contents: olivine, fayalite, and forsterite. Fayalite is the iron endmember and forsterite the magnesium endmember of the olivine group ( $(\text{Mg}, \text{Fe})_2\text{SiO}_4$ ).

Optical constants of minerals of the olivine group have already been published (Steyer 1974 (Mg-rich olivine); Hofmeister 1997 (fayalite); Servoin & Piriou 1973 (forsterite); Iishi 1978 (forsterite)). For forsterite and an Mg-rich olivine, we improve the quality of the data by a broader wavelength coverage and the higher spectral resolution of our measurements, respectively. We identify certain additional vibrational modes in the spectra. The optical constants of fayalite are reconsidered on the basis of our new reflection measurements. We find deviations from

Send offprint requests to: D. Fabian,  
e-mail: [fabian@astro.uni-jena.de](mailto:fabian@astro.uni-jena.de)

the data published by Hofmeister (1997) in terms of band strengths.

In contrast to amorphous silicates, crystalline silicates have a lot of diagnostic bands due to metal-oxygen vibrations. Emission features of crystalline silicates have been observed in numerous astrophysical environments. Evidence for the presence of magnesium-rich crystalline olivines and pyroxenes have been found in circumstellar regions (envelopes/disks) around young and evolved stars, IDPs, comets, and in meteorites (see, e.g., for AGB stars: Molster et al. 1999; planetary nebulae: Waters et al. 1996, Beintema 1998, Cohen et al. 1999, Molster 2000, Lim et al. 2001; Orion nebula and the HII region M17-SW: Cox & Roelfsema 1999, Cesarsky et al. 2000, Molster 2000; circumstellar disks surrounding Herbig Ae/Be stars: Malfait et al. 1998, Malfait et al. 1999 (HD 100546), Waelkens et al. 2000 (HD142527), Meeus et al. 2001; IDPs: Sandford & Walker 1985, Sandford & Walker 1985, Bradley 1995, Bradley et al. 2000; comets: Hanner 1999, Crovisier et al. 1997, Wooden et al. 1999). Fayalite has not been observed in circumstellar shells so far. However, fayalite has been found in the matrix of a chondritic meteorite indicating a vapour growth prior to parent body accretion (Weisberg et al. 1997).

Silicates are assumed to condense in the ejecta of evolved stars mainly in an amorphous state. However, at high temperature, a certain percentage can also condense as manifoldly shaped nanocrystals as was shown by condensation experiments (Tsuchiyama 1998). Initially amorphous silicates can also transform into an ordered crystalline structure by the process of thermal annealing at sufficiently high temperature (Gail & Sedlmayr 1998). Annealing experiments have been performed by Hallenbeck et al. (1998), Brucato et al. (1999), and Fabian et al. (2000).

The aim of this paper is to provide optical constants of crystalline silicates of olivine composition ranging from forsterite to fayalite. The composition and homogeneity of the materials were characterized by scanning electron microscopy (SEM) and energy dispersive X-ray analysis (EDX) (see Sect. 2). Section 3 presents the reflection spectra and the derived optical data. In Sect. 4, morphological effects as well as the influence of the matrix on band profiles and absolute absorption efficiencies will be outlined. Finally, the results of this study are used to discuss the recent band identifications of crystalline dust features in ISO spectra.

## 2. Experimental procedure

### 2.1. Spectroscopy

Infrared spectra of the relevant materials have been obtained using a Bruker FTIR spectrometer (IFS 113v) for wavelengths between 2 and 200  $\mu\text{m}$  ( $5000\text{--}50\text{ cm}^{-1}$ ). Measurements in the mid-infrared (MIR:  $5000\text{--}400\text{ cm}^{-1}$ ) and in the far-infrared spectral range (FIR:  $700\text{--}50\text{ cm}^{-1}$ ) were performed using a KBr and a mylar beamsplitter,

respectively. According to this, the overlap amounts to  $300\text{ cm}^{-1}$ . Finally, the spectra were merged without an offset or scaling. The resolution of the measurements was  $2\text{ cm}^{-1}$ . This medium resolution has been proven to be sufficient for room temperature measurements in order to resolve all bands (Bowey et al. 2001). The specular reflectance spectra, at nearly normal incidence, have been measured using a gold mirror as reference. Single crystals were crystallographically oriented by Laue diffraction, embedded in an epoxy resin and polished for reflectance spectroscopy. Since olivines belong to the orthorhombic crystallographic system, for each of the crystals three reflection measurements with radiation polarized along the three different crystallographic directions had to be performed. MIR and FIR grating polarizers have been used for producing polarized IR radiation.

Transmission spectra of small particles ( $d < 1\text{ }\mu\text{m}$ ) have been recorded using the well-known KBr/PE pellet technique (see, e.g., Jäger et al. 1994; Henning & Mutschke 2000). For these measurements, small grains with sizes clearly less than  $1\text{ }\mu\text{m}$  were produced by grinding of crushed single crystals in a planetary mill for 1 h. Large grains were removed by sedimentation in ethanol.

### 2.2. Forsterite

In the case of forsterite we measured the reflectivity on polycrystalline material in the FIR. The goal of these measurements was to find additional fundamental lattice vibrations predicted by group theory (Iishi 1978), but not present in the data published by Servoin & Piriou (1973). The polycrystalline forsterite has been produced from a mixture of  $\text{MgCO}_3$  and  $\text{SiO}_2$  powders in the right stoichiometry. The melts were kept at 2023 K for 10 min and subsequently cooled down ( $\approx 1000\text{ K/h}$ ) to room temperature. XRD analyses proved that the oxides transformed into forsterite quantitatively. SEM investigations have demonstrated that the sample consists of crystallites with sizes less than  $1\text{ }\mu\text{m}$ .

### 2.3. Olivine

Spectroscopy was performed using an Mg-rich natural single crystal (from Stubachtal, Pinzgau, Austria) with the composition  $\text{Mg}_{1.9}\text{Fe}_{0.1}\text{SiO}_4$ . The crystal has thoroughly been investigated by SEM combined with EDX and XRD (X-Ray Diffraction) analysis. The Laue diffraction proved that the used sample was indeed a single crystal.

### 2.4. Fayalite

Fayalite single crystals have been grown by the scull method where 1–2 kg of polycrystalline fayalite material was inductively molten and slowly cooled in a sinter crust crucible under a defined oxygen partial pressure (Lingenberg 1986). This method provides fayalite single crystals up to a size of about 6 mm. The crystals have

been analysed by XRD and turned out to consist entirely of fayalite without any inclusions of  $\text{SiO}_2$ , metallic iron or iron oxides.

### 3. Results

Optical constants  $n$  and  $k$  have been derived from the polarized reflectance spectra of bulk samples ( $R = [(n-1)^2 + k^2] / [(n+1)^2 + k^2]$ , Bohren & Huffman 1983). For each of the materials three sets of optical constants have been determined from the polarized reflection spectra. These spectra correspond to the vibrational directions parallel to the three crystallographic axes  $x$ ,  $y$  and  $z$ . To derive the dielectric function  $\epsilon(\nu)$  from the reflectance spectra, we relied on the classical Lorentz oscillator model, according to which the dielectric function  $\epsilon(\nu)$  is given by:

$$\epsilon(\nu) = \epsilon_\infty + \sum_j \frac{\Omega_j^2}{\nu_j^2 - \nu^2 - i\gamma_j\nu} \quad (1)$$

where  $\Omega_j^2$  is the respective oscillator strength,  $\gamma_j$  the damping constant, and  $\nu_j$  the resonance frequency of the  $j$ th oscillator. According to group theory, the forsterite and fayalite lattice structure is characterized by 35 infrared active modes (9  $B_{1u}$  ( $E||z$ ), 13  $B_{2u}$  ( $E||y$ ), 13  $B_{3u}$  ( $E||x$ ); Servoin & Piriou 1973). Assignments of the modes to vibrations of metal-oxygen bondings and  $\text{SiO}_4$  tetrahedra have already been performed by Iishi (1978).

#### 3.1. Forsterite

Our powder absorption and reflection spectra of polycrystalline forsterite showed two additional FIR features at  $143.3$  and  $200.8 \text{ cm}^{-1}$ , which were not found in previous reflection measurements performed by Servoin & Piriou (1973). The FIR range was not covered in the reflection measurements performed by Iishi (1978). The presence of the two new bands were theoretically predicted by group theoretical analysis at positions between  $135$  and  $140$  ( $B_{2u}$ ) and  $183$  and  $209 \text{ cm}^{-1}$  ( $B_{1u}$ ,  $B_{3u}$ ), respectively (Iishi 1978). Indications for these bands were already found in powder measurements of Ochler et al. (1969).

To get optical constants over a broad wavelength range, we combined our FIR measurements with the optical constants published by Servoin & Piriou (1973). We did not use the Iishi (1978) data because he did not explicitly show the reflection spectra and covered a shorter wavelength range only.

The oscillator wavenumber positions, the oscillator strengths, and the damping constants of the two new features have been estimated from a fit of our reflection spectra of polycrystalline forsterite ( $B_{2u}$ :  $\nu = 143.3 \text{ cm}^{-1}$ ,  $\Omega = 35 \text{ cm}^{-1}$ ,  $\gamma = 5 \text{ cm}^{-1}$ ;  $B_{1u}$ ,  $B_{3u}$ :  $\nu = 200.8 \text{ cm}^{-1}$ ,  $\Omega = 29 \text{ cm}^{-1}$ ,  $\gamma = 5 \text{ cm}^{-1}$ ).

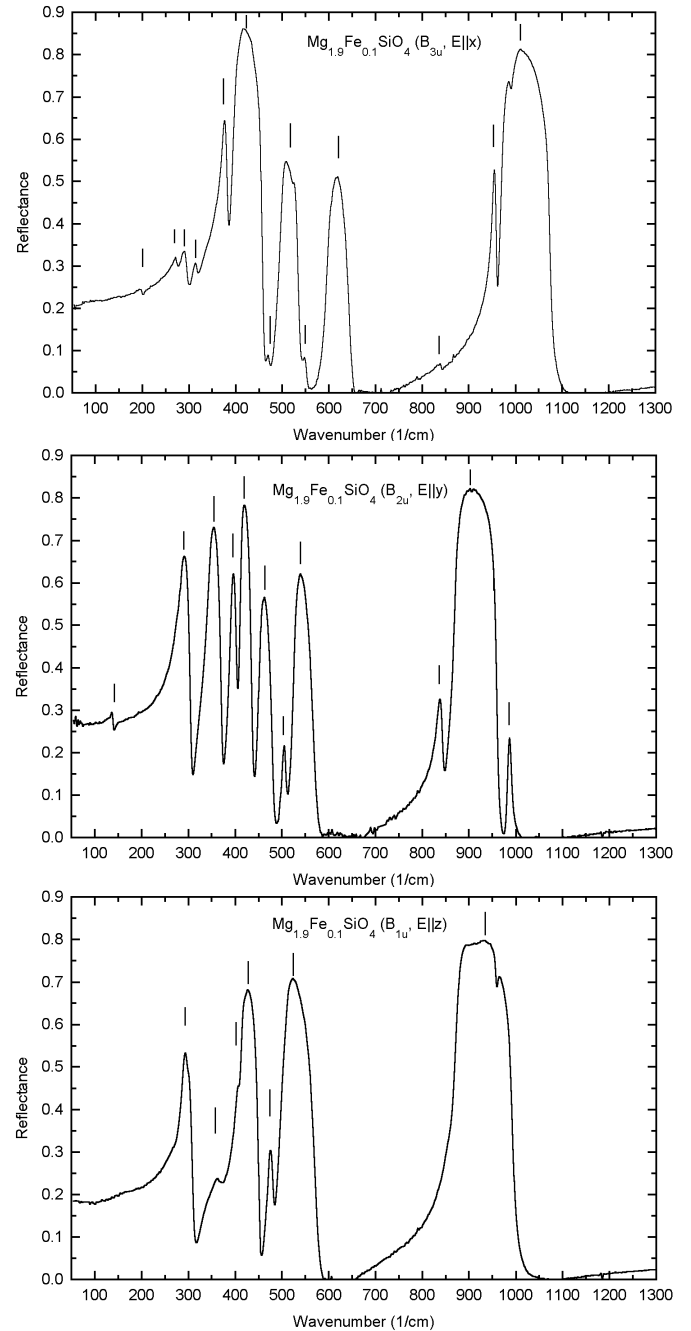


**Fig. 1.** Polarized reflectance spectra of a natural olivine single crystal in the IR ( $E \parallel x$ ,  $E \parallel y$  and  $E \parallel z$ ,  $\mathbf{E}$  being the electrical vibration vector). Lattice vibration bands are indicated by vertical dashes.

#### 3.2. Mg-rich olivine

Figure 2 shows the complex refractive index  $n + ik$  of the Mg-rich olivine derived from the IR reflectance spectra (Fig. 1). Instead of 35 theoretically expected modes, 31 (7  $B_{1u}$ , 11  $B_{2u}$ , and 13  $B_{3u}$ ) lattice modes could be resolved. The reflection spectra have been compared with the reflection measurements performed by Steyer (1974), who observed only 26 of the 35 predicted bands. With the exception of the bands not resolved by Steyer (1974), there is a good agreement between the positions and strengths

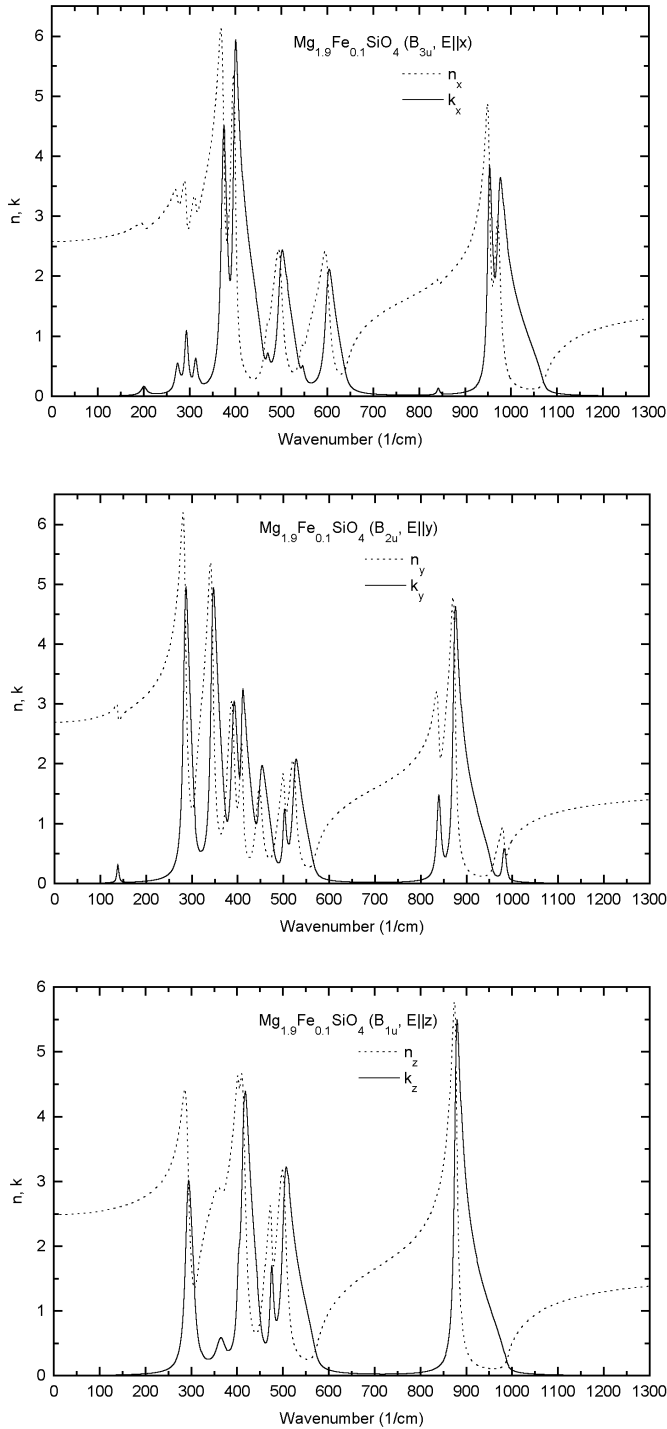


**Fig. 2.** Complex refractive index  $n + ik$  of an olivine single crystal in the IR ( $E \parallel x$ ,  $E \parallel y$  and  $E \parallel z$ , resp.).

of the features present in both measurements of the reflectivity.

Group theoretical analysis (Iishi 1978) predicts that only one  $B_{1u}$  mode should occur in the  $10 \mu\text{m}$  region. The weak feature at the blue wing of the strong band (see Fig. 1) is an overtone and was not considered in the fitting procedure.

### 3.3. Fayalite

Using the reflectance spectra (see Fig. 3), the complex refractive indices were calculated by fitting the spectra with oscillators (see Fig. 4). In contrast to the theoretically predicted 35 modes, only 28 lattice modes (7  $B_{1u}$ , 10  $B_{2u}$ , and 11  $B_{3u}$ ) have been resolved. The measured reflectance spectra of fayalite (see Fig. 3) are partly in good agreement with those published by Hofmeister (1997) with respect to the number, positions and strengths of the reflection bands. However, the measured reflectance values in the  $10 \mu\text{m}$  range are significantly higher (about 15%) in our measurements compared to the data published by Hofmeister (1997). In addition, she found overtones which are not present in our data. The differences cause stronger deviations in the optical constants. In detail, our resonances are significantly stronger in the  $10 \mu\text{m}$  range. Hofmeister (1997) reported the observation of two additional FIR lattice modes at  $86 \text{ cm}^{-1}$  ( $B_{2u}$ ) and at  $106 \text{ cm}^{-1}$  ( $B_{1u}$ ), only measured at thin sections, which could not be resolved in our measurements.

## 4. Discussion

By comparing Figs. 1 to 4, we can easily see that Mg-rich and Fe-rich silicates have bands at different positions and wavenumbers. This is less true for the bending and stretching vibrations of the  $\text{SiO}_4$  tetrahedra. For the other bands, the features are shifted to smaller wavenumbers in the case of Fe-rich silicates simply because the cation mass is higher. This is in agreement with earlier results obtained with transmission measurements (Jäger et al. 1998).

In the following, we will calculate mass absorption coefficients (MACs)  $\kappa$  from the optical constants. We consider different shapes and shape distributions of the particles. These data are needed for the direct comparison with astronomical measurements. In the optically thin case, measured fluxes are directly proportional to MACs. For other configurations, the MACs are required to perform radiative transfer calculations. Therefore, we give all these data on a wavelength scale (instead of a wavenumber scale).

Furthermore, we will use the calculated MAC spectra to evaluate MACs obtained directly from transmission measurements of material embedded in a KBr or polyethylene (PE) matrix.

We will consider randomly oriented ellipsoids, spheres, and two continuous distributions of ellipsoids (Ossenkopf, private communication) in the Rayleigh limit. The continuous distributions of ellipsoids are characterized either by equal probability of all shapes (CDE1) or by a quadratic weighting, where near-spherical particle shapes are most probable (CDE2). The relevant formulae are given in Eqs. (2)–(6). Here,  $Q_{\text{ext}}$  is the extinction cross section,  $\rho$  the material density and  $a$  the particle radius (for ellipsoids it is equivalent to the radius of a sphere with the same volume). The quantities  $\epsilon$  and  $\epsilon_m$  are the

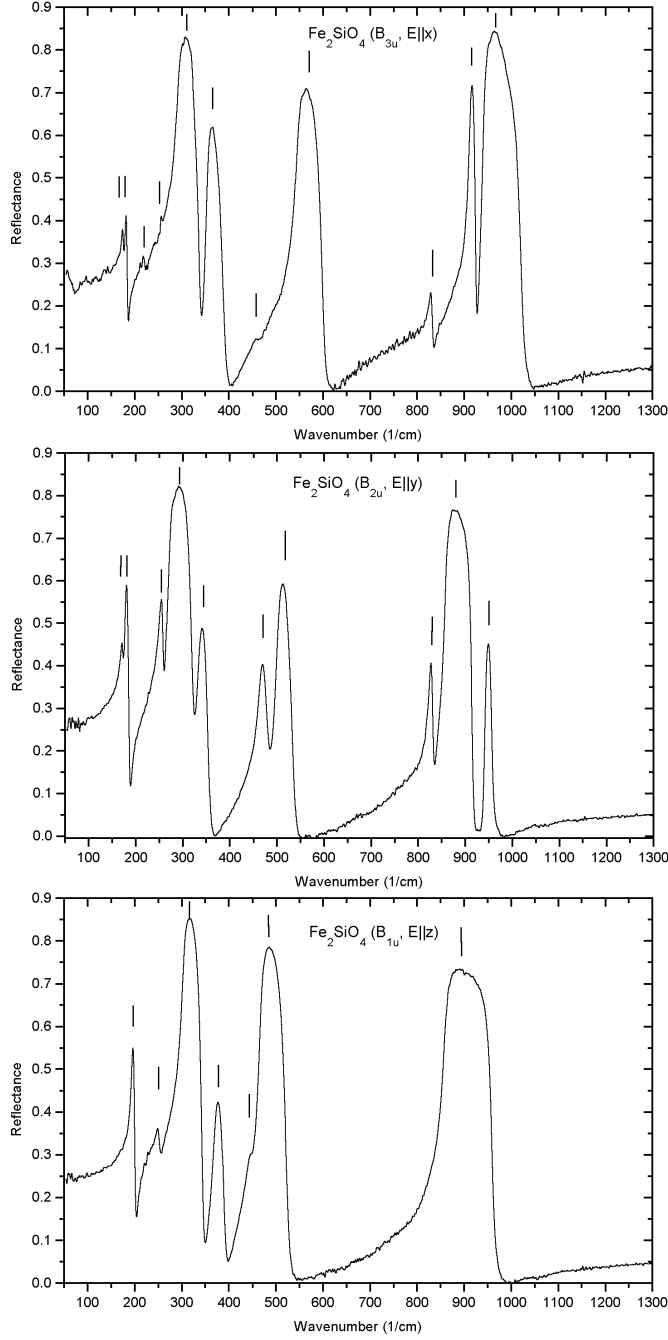


**Fig. 3.** Polarized reflectance spectra of a fayalite single crystal ( $E \parallel x$ ,  $E \parallel y$  and  $E \parallel z$ , resp.). Lattice vibration bands are indicated by vertical dashes.

complex dielectric function of the material and the dielectric constant of the non-absorbing surrounding medium.  $V = 4\pi abc/3$  is the volume of the ellipsoid with  $a$ ,  $b$ , and  $c$  as the principal axes of the ellipsoid. The quantity  $k = 2\pi\sqrt{\epsilon_m}/\lambda$  is the wave vector. Note that the equation for spheres is contained in Eq. (2) for  $L_i = 1/3$ .

$$C_{\text{ext}}(\text{ell}) = \frac{kV}{3} \text{Im} \left[ \sum_{i=1}^3 \frac{\epsilon - \epsilon_m}{\epsilon_m + L_i(\epsilon - \epsilon_m)} \right], \quad \sum_{i=1}^3 L_i = 1 \quad (2)$$

$$C_{\text{ext}}(\text{sphere}) = 3kV \text{Im} \left[ \frac{\epsilon - \epsilon_m}{\epsilon + 2\epsilon_m} \right], \quad (3)$$

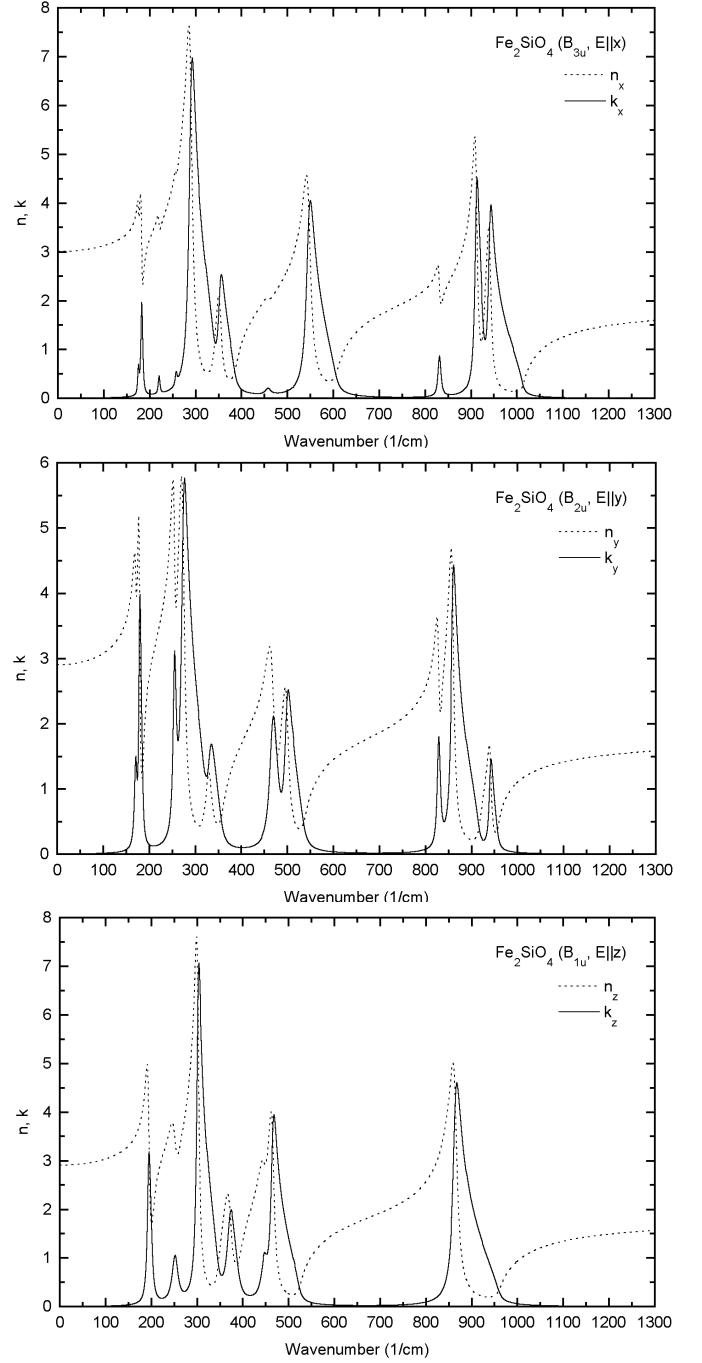


**Fig. 4.** Complex refractive index  $n + ik$  of a fayalite single crystal ( $E \parallel x$ ,  $E \parallel y$  and  $E \parallel z$ , resp.).

$$C_{\text{ext}}(\text{CDE1}) = 2kV \text{Im} \left[ \frac{\epsilon}{\epsilon - \epsilon_m} \ln \left( \frac{\epsilon}{\epsilon_m} \right) \right], \quad (4)$$

$$C_{\text{ext}}(\text{CDE2}) = 20kV \text{Im} \left[ -\frac{\epsilon^3 \epsilon_m}{(\epsilon - \epsilon_m)^4} \ln \left( \frac{\epsilon}{\epsilon_m} \right) + \frac{\epsilon_m^3}{(\epsilon - \epsilon_m)^3} + \frac{5\epsilon_m^2}{2(\epsilon - \epsilon_m)^2} + \frac{11\epsilon_m}{6(\epsilon - \epsilon_m)} + \frac{1}{4} \right], \quad (5)$$

$$\kappa = \frac{C_{\text{ext}}}{V\rho}. \quad (6)$$

Since olivine is an anisotropic mineral, the extinction coefficient of olivine particles depends on the alignment of the crystallographic axis. For anisotropic ellipsoids which axes coincide with the crystallographic axes, the anisotropy can analytically be taken into account. The Eq. (2) transforms into

$$C_{\text{ext}}(\text{ell}) = \frac{kV}{3} \text{Im} \left[ \sum_{i=1}^3 \frac{\epsilon_i - \epsilon_m}{\epsilon_m + L_i(\epsilon_i - \epsilon_m)} \right], \quad \sum_{i=1}^3 L_i = 1 \quad (7)$$

where  $\epsilon_i$  stands for  $\epsilon_{x,y,z}$ . These transformations have also to be applied to the equations for spheres and distributions of ellipsoids. The anisotropic sphere is a special case of an anisotropic ellipsoid and therefore contained in Eq. (7). The averaging can also be applied to the CDEs, at least if only ellipsoids with axes parallel to the crystallographic axes are considered. Generally, the procedure corresponds to an averaging according to

$$C_{\text{ext}} = \frac{1}{3} [C_{\text{ext}}(\epsilon_x) + C_{\text{ext}}(\epsilon_y) + C_{\text{ext}}(\epsilon_z)]. \quad (8)$$

#### 4.1. Evaluation of transmission measurements

In the astronomical literature, a long and somewhat controversial discussion concerning possible “KBr matrix effects” exists (see, e.g., Papoular et al. 1998; Henning & Mutschke 2000; Speck et al. 2000 for discussions and references). Such effects may be of importance when the transmission of light through a KBr/PE pellet with embedded small particles is measured. There is no doubt from fundamental electromagnetism that the absorption and scattering efficiencies of small particles depend on the refractive index of the surrounding medium (Bohren & Huffman 1983, see Eqs. (2)–(5)). We should also note that clumping of particles and grain boundaries may exist in a pellet, thereby influencing the scattering behaviour.

MACs for spheres and CDEs of forsterite have been calculated for particles in the Rayleigh limit, which are embedded in a KBr or PE matrix ( $\epsilon_m = 2.25$ ). The results of these calculations are compared with the transmission measurements on small particles ( $d < 1 \mu\text{m}$ ) dispersed in KBr and PE (see Fig. 5). These calculations demonstrate that the CDE1 results agree relatively well with the powder measurements. In detail, the comparison shows a good agreement of the peak positions with CDE1 (see also Zubko et al. 1996). This is a consequence of the production of small irregularly-shaped particles by mechanical grinding, a process which finally leads to rather irregular grain shapes. However, the maximum absorption values of the measured samples are significantly lower compared to calculations in the medium. This indicates that particles with sizes of about  $1 \mu\text{m}$  are close to but not in the Rayleigh limit, at least not in the strong bands. Additionally, the continuum obtained from the transmission measurements is enhanced compared to the values based on the reflection measurements in regions where the MACs are small. The latter behaviour is probably caused by particle agglomeration/boundaries in the matrix or a not optimal calibration

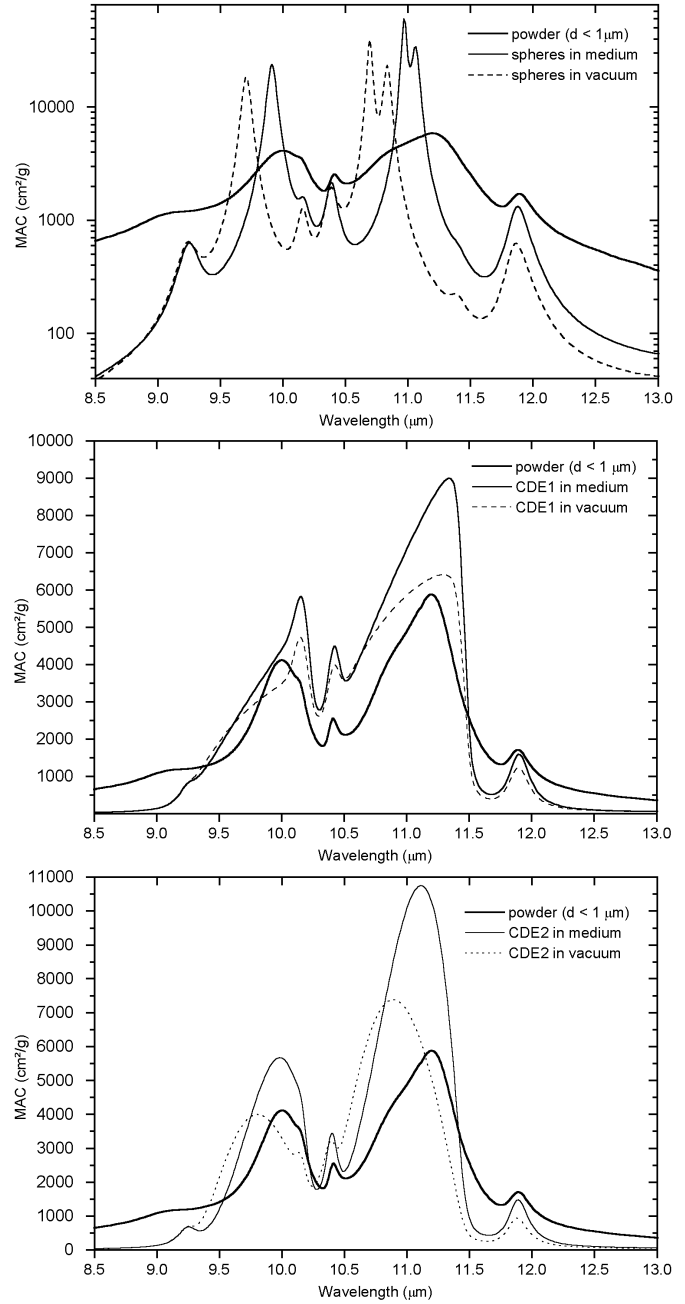


**Fig. 5.** MACs of forsterite spheres, CDE1, CDE2 in a surrounding medium of  $\epsilon_m = 2.25$  that is valid for KBr and PE in the IR range compared to vacuum. The particles are in the Rayleigh limit. Additionally, the calculations are compared to powder ( $d < 1 \mu\text{m}$ ) transmission measurements dispersed in KBr/PE.

of the scattering by the pellet. This fact should serve as a warning that MACs from transmission measurements may overestimate the true values of a low continuum.

In general, the strongest features show the most pronounced change of the band shape. Since the real part of the dielectric function does not approach zero for the small features in the FIR, the bands remain practically unaffected.

## 4.2. Comparison with the observations

### 4.2.1. Calculations and lattice mode assignments

MACs for spheres and CDEs of forsterite, fayalite and olivine have been calculated for particles in vacuum (Figs. 6–8). These simple models for particle shapes are chosen in order to show the dependence of peak positions on particle shape and iron content. For completeness, the powder spectra of small particles ( $d < 1 \mu\text{m}$ ) of the materials dispersed in KBr/PE are also plotted in the figures. However, they will not be used for the comparison with astronomical data. The peak positions for all three silicate minerals extracted from the sphere calculations are summarized in Table 1. The table shows that the bands shift considerably with increasing Fe/Mg-ratio. As was already outlined for the reflectance spectra, the peak positions are shifted towards longer wavelengths with increasing iron content from forsterite to fayalite due to the increasing bonding lengths between oxygen and magnesium or iron atoms and higher atomic mass of the iron atom (Jäger et al. 1998). Additionally, the assignments of the bands to the fundamental lattice vibrational modes are given in Col. 4. Peak positions assigned to identical lattice vibration modes are given in one line. In order to compare our experimental results with observed astronomical spectra, the comprehensive analysis of spectral features of circumstellar dust performed by Molster (2000) was used. This analysis employed all ISO spectra available for optically thin dust shells of oxygen-rich evolved stars. A number of bands were attributed to forsterite by Molster (2000). In Fig. 6, the wavelength intervals of these bands are marked by vertical bars and the average wavelength positions of the observed features are given. The comparison of the peak positions of the MAC spectra with the observationally-based positions shows that the observed peak positions are somewhat longward to that of spheres. Certain features, such as the  $11.4 \mu\text{m}$  feature cannot be explained by spheres at all. It turns out that the best agreement for most band positions is achieved by the CDE1. However, a few exception can be identified, such as the  $9.8 \mu\text{m}$  feature, that is best matched by an absorption maximum produced by spheres. Here we should note again that the weaker FIR bands are *not* strongly influenced by shape effects.

### 4.2.2. Elongated particle shapes

The comparison of the MACs to the observations revealed that the observed band positions are better reproduced by a wide distribution of ellipsoidal shapes (CDE1) than by spherical grains. However, the calculated band widths for the CDE1 are too broad in relation to the widths of the observed silicate bands. This fact leads to the consideration of special ellipsoidal shapes including elongated ones, which produce bands at the position of the CDE1 peak but with much smaller width.

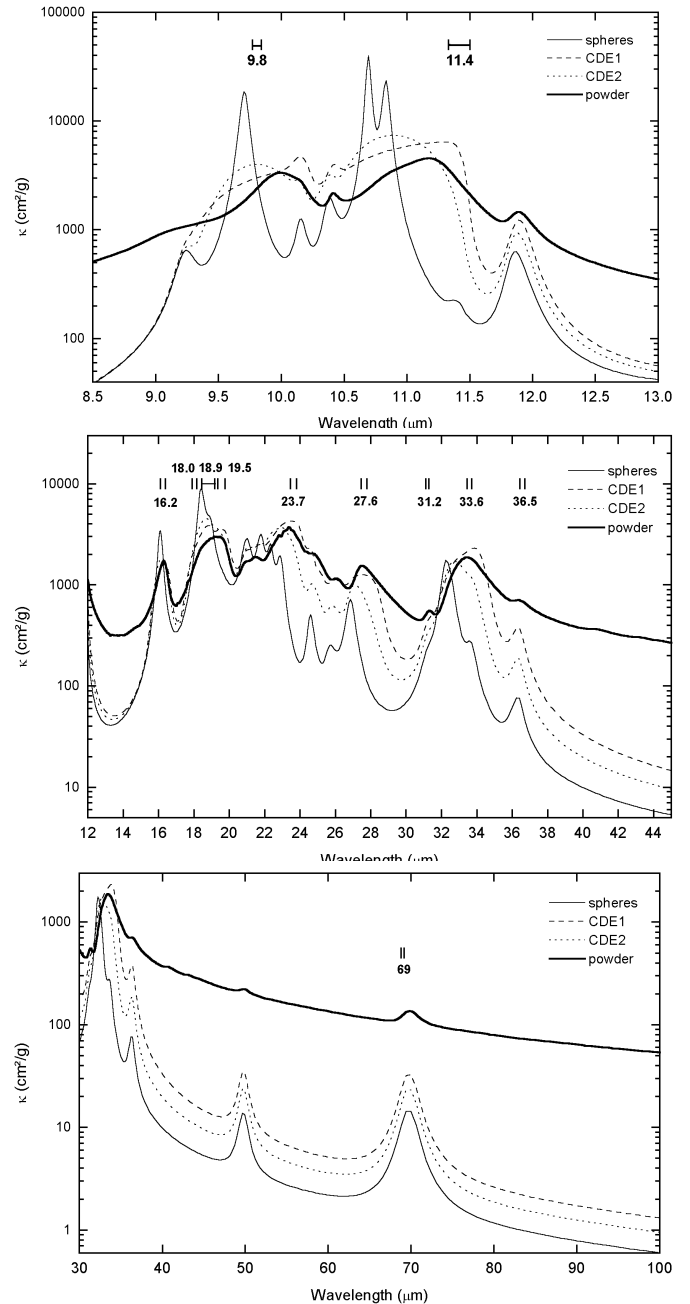


**Fig. 6.** MACs of forsterite spheres, CDE1, CDE2 in vacuum in the Rayleigh limit, and powder ( $d < 1 \mu\text{m}$ ) dispersed in KBr/PE. Peak positions assigned to forsterite from Molster (2000) have been indicated. The spectra are presented in three figures for clarity.

The shape distribution of particles in space is practically unknown although the interstellar polarization points to the presence of elongated particles in the diffuse interstellar medium. In this context, we note that condensation experiments show indeed the formation of elongated forsterite crystals.

In such experiments performed by Tsuchiyama (1998), the formation of nanocrystals resembling euhedral flakes is found at the onset of silicate condensation at high temperature. The crystals had manifold shapes, depending

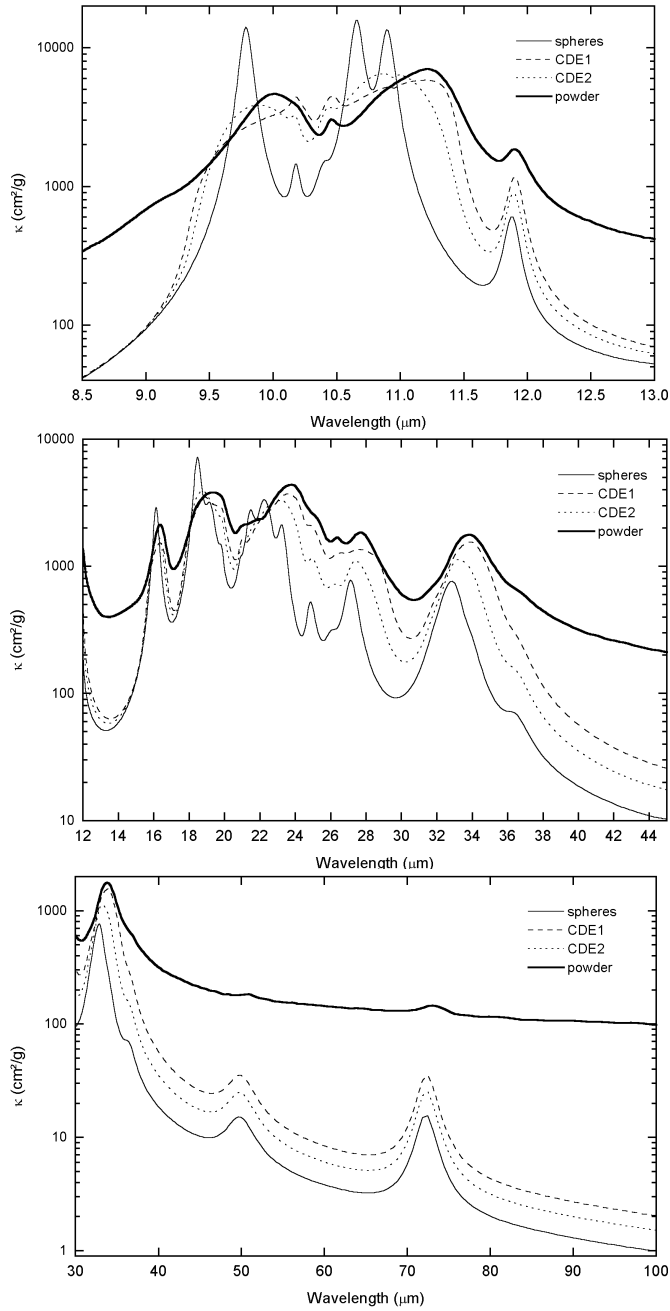


**Fig. 7.** MACs of olivine spheres, CDE1, CDE2 in vacuum in the Rayleigh limit, and powder ( $d < 1 \mu\text{m}$ ) dispersed in KBr/PE. The spectra are presented in three figures for clarity.

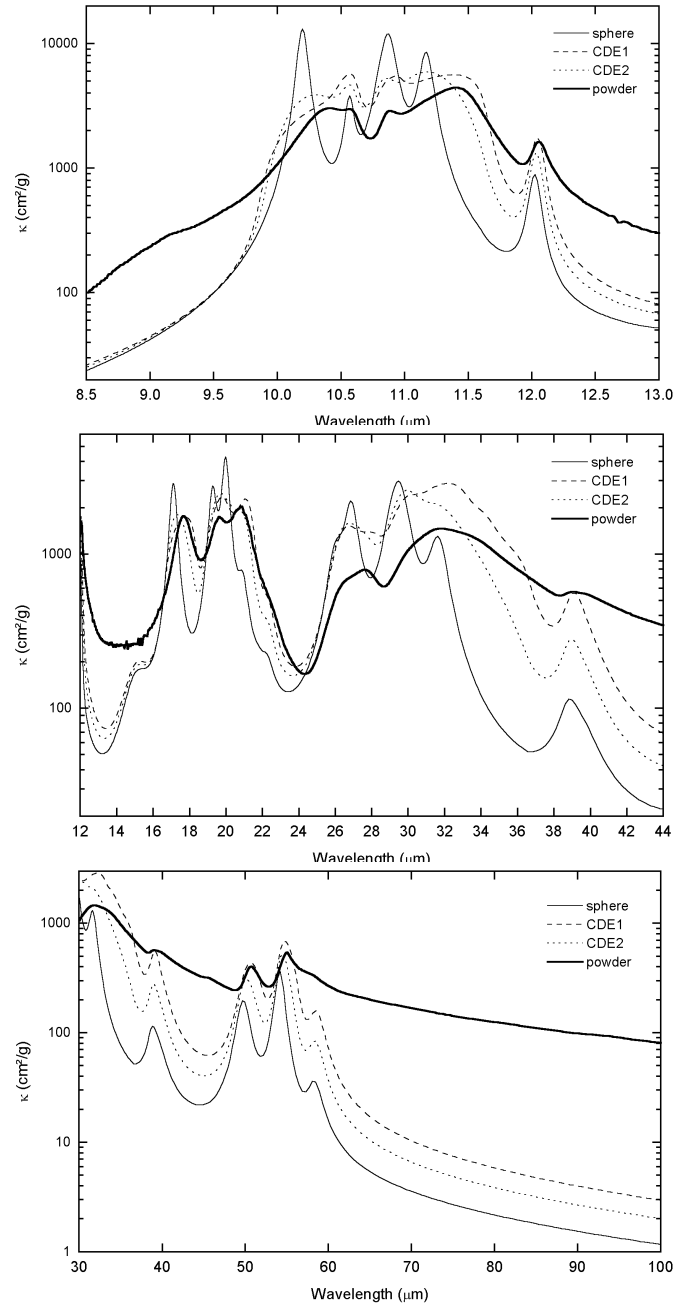


**Fig. 8.** MACs of fayalite spheres, CDE1, CDE2 in vacuum in the Rayleigh limit, and powder ( $d < 1 \mu\text{m}$ ) dispersed in KBr/PE. The spectra are presented in three figures for clarity.

on condensation temperature. Their shapes are characterized by an elongation along the  $c$ -axis (Tsuchiyama 1998). At lower temperatures, silicates condense in the amorphous state and with spherical shape (Fabian et al. 2000). However, also these particles can develop a crystalline structure by annealing processes.

For these reasons, in the following, we assume the forsterite dust component to consist of both spherical particles and of crystals elongated along the  $c$ -axes ( $c$ -elongated ellipsoids).

We compare again the results of these calculations with the band positions of circumstellar dust features given by Molster (2000). This comparison is shown in Fig. 9.

**10 micron complex (7–13  $\mu\text{m}$ ):** The comparison with calculations for spheres and shapes elongated along the  $c$ -axes indicate that the 9.4 and 11.4  $\mu\text{m}$  features are pronounced for very elongated ellipsoids, whereas the 9.8  $\mu\text{m}$  feature indicates the existence of sphere-like grains. Additionally, the 10.7  $\mu\text{m}$  emission feature, assigned by Molster (2000)

**Table 1.** Peak positions of forsterite ( $\text{Mg}_2\text{SiO}_4$ ), olivine ( $\text{Mg}_{1.9}\text{Fe}_{0.1}\text{SiO}_4$ ) and fayalite ( $\text{Fe}_2\text{SiO}_4$ ) determined from MAC calculations of spheres in vacuum (Rayleigh limit,  $\lambda$  in  $\mu\text{m}$ ). Identical lattice modes are given in one line.

Forsterite	Olivine	Fayalite	Assignment
9.24	-	-	$B_{2u}$ : overtone (*)
9.70	9.78	10.20	$B_{3u}$ : $\nu_3$
10.15	10.18	10.56	$B_{2u}$ : $\nu_3$
10.38	10.43	10.88	$B_{3u}$ : $\nu_3$
10.70	10.88	10.88	$B_{1u}$ : $\nu_3$
10.86	sh.	11.17	$B_{2u}$ : $\nu_3$
11.86	11.88	12.03	$B_{2u}$ : $\nu_1$ , $B_{3u}$ : $\nu_1$
16.08	16.14	17.11	$B_{3u}$ : $\nu_4$
18.43	18.50	19.27	$B_{2u}$ : $\nu_4$
18.43	18.50	19.98	$B_{1u}$ : $\nu_4$
18.92	19.18	22.22	$B_{3u}$ : $\nu_4$
19.5	19.80	20.85	$B_{2u}$ : $\nu_4$
21.00	20.88	22.22	$B_{1u}$ : $\nu_2$
21.00	21.44	29.46	$B_{2u}$ : $\nu_2$
21.79	22.26	26.88	$B_{3u}$ : $\nu_2$
22.32	22.55 sh.	26.0	$B_{1u}$ : $R(\text{SiO}_4:y)$
22.87	23.25	31.62	$B_{2u}$ : $R(\text{SiO}_4:z)$
24.63	24.86	38.80	$B_{2u}$ : $T(\text{MI}:z)$
25.70	26.07	38.80	$B_{3u}$ : $T(\text{MI}:z)$
26.86	27.11	38.80	$B_{2u}$ : $T(\text{MII}:x, y)$
31.2 sh.	31.77 sh.	45.30	$B_{3u}$ : $T(\text{MI}:z, y)$
32.28	32.63	49.7	$B_{1u}$ : $T(\text{MI}:z)$
32.28	32.97	54.2	$B_{2u}$ : $T(\text{MI}:x, z; \text{MII}:y)$
33.59	33.90 sh.	54.2	$B_{3u}$ : $T(\text{MI}:z, z)$
36.30	36.5	58.30	$B_{1u, 2u, 3u}$ : $T(\text{MII})$ (*)
49.9	49.8	94.34 (f)	$B_{3u}$ : $T(\text{MI}, \text{SiO}_4:y)$ (*)
			$B_{3u}$ : $T(\text{MI}, \text{SiO}_4:y)$ (*)
69.9	72.5	116.28 (f)	$B_{2u}$ : $T(\text{MII}, \text{SiO}_4:x)$ (*)

(f) means that the feature was observed in thin section measurements performed by Hofmeister (1997). sh. means shoulder. Assignments according to Ishi (1978) and Hofmeister (1987):  $T(\text{SiO}_4:x)$  translation of the  $\text{SiO}_4$  tetrahedron;  $R(\text{SiO}_4:x)$  rotation of the  $\text{SiO}_4$  tetrahedron;  $T(\text{MI}:x)$ , translation of the divalent cation MI;  $\nu_4$  asymmetric bending vibration of tetrahedron;  $\nu_3$  asymmetric stretching vibration of tetrahedron;  $\nu_2$  symmetric bending vibration of tetrahedron;  $\nu_1$  symmetric stretching vibration of tetrahedron; (\*) most probable assignment.

to enstatite could also be caused by both forsterite spheres and nanocrystals elongated along the  $c$ -axis (see Fig. 9a).

**18 micron complex (15–21  $\mu\text{m}$ ):** Molster (2000) reported two features at 15.9 and 16.2  $\mu\text{m}$ . Both features can be caused by forsterite nanocrystals, the 15.9  $\mu\text{m}$  band by

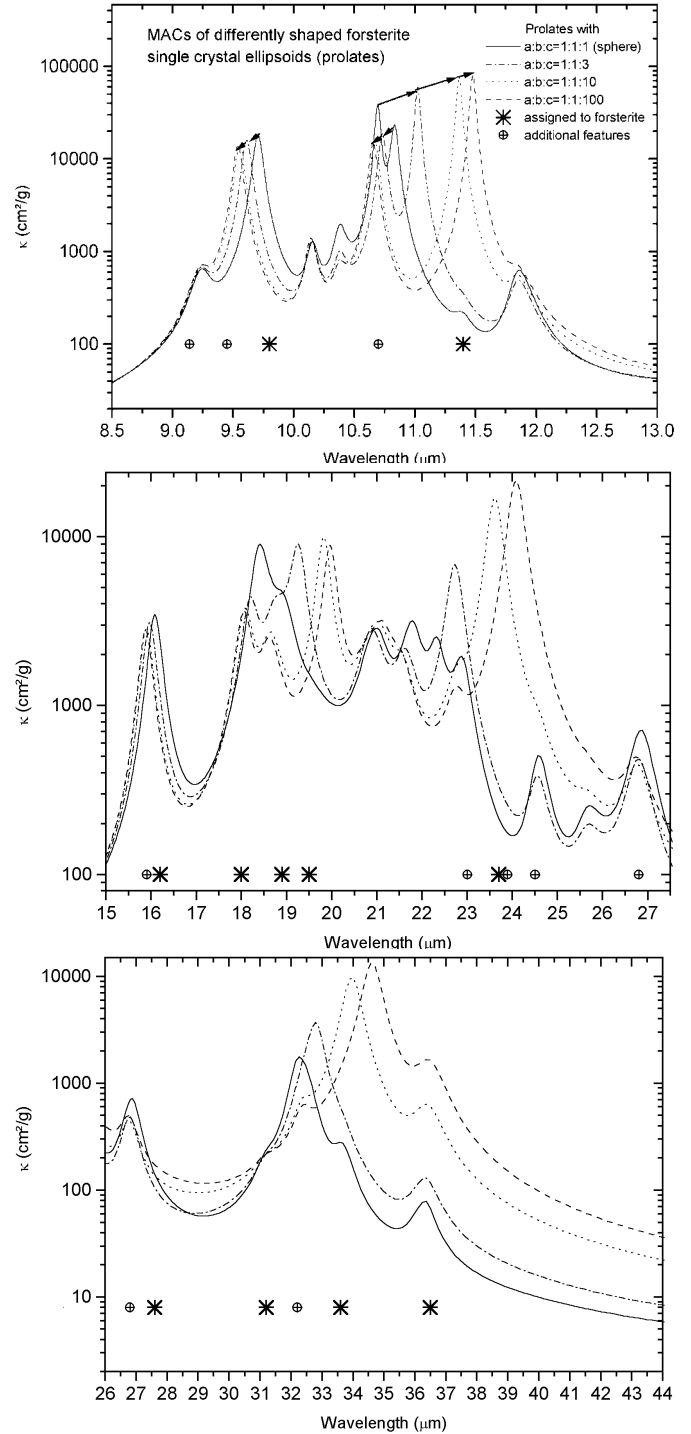


**Fig. 9.** MACs of forsterite ellipsoids elongated along the  $c$ -axis in vacuum in the Rayleigh limit. Peak positions assigned to forsterite and additional features that can be assigned to forsterite have been indicated (from Molster 2000). In the 10  $\mu\text{m}$  range, the peak shifts from spheres to needles are indicated by arrows as an example.

$c$ -elongated needles and the 16.2  $\mu\text{m}$  band by spheres. The range from 18 to 19.5  $\mu\text{m}$  is characterized by a couple of strong features, that can be caused by sphere-like forsterite crystals (CDE2) dominating the 18  $\mu\text{m}$  feature and  $c$ -elongated ellipsoids emitting in the 19  $\mu\text{m}$  range.

However, the  $c$ -elongated ellipsoids show strong features at 20  $\mu\text{m}$  that are not observed.

**23 micron complex (22–25.5  $\mu\text{m}$ ):** Ellipsoids elongated along the  $c$ -axes show very strong features ranging from 22.5  $\mu\text{m}$  for sphere-like particles to 24  $\mu\text{m}$  for  $c$ -needles. For this reason, the observed feature can be caused by an distribution of such  $c$ -elongated shapes. A feature at 24.5  $\mu\text{m}$  can be assigned to spheres.

**28 micron complex (26–32  $\mu\text{m}$ ):** Molster (2000) reports features at 26.8 and 31.2  $\mu\text{m}$  that are present in spectra of both spheres and  $c$ -ellipsoids. The other observed features in this range cannot be caused by forsterite spheres or  $c$ -elongated ellipsoids.

**32–100 micron range:** The observations show strong features at 32.2, 32.8, 32.97 and 33.6  $\mu\text{m}$ . The feature at 32.2  $\mu\text{m}$  can be assigned to spheres, the feature at 33 and 34  $\mu\text{m}$  could be caused by somewhat  $c$ -elongated ellipsoids. However, the resonance of  $c$ -needles shows the peak at 35  $\mu\text{m}$ , that is too longward. The 36.6, 49, and 69  $\mu\text{m}$  features are present in spectra of all shapes of forsterite particles.

#### 4.2.3. Band widths and temperature effects

The narrowness of the observed crystalline bands seems to indicate that the dust particles have a narrow shape distribution. In this context, Table 2 shows that band widths for the CDEs are too broad in relation to those of the observed bands. Only spheres or special ellipsoidal shapes can produce sufficiently narrow features for most of the bands. A few of the weaker observed features show in some objects even smaller  $FWHM$ s (Full Width of Half Maximum) than the calculated  $FWHM$ s of spheres. If this is true, there remains the possibility that these features are caused by other carriers. Another explanation might be that the dielectric function derived from bulk laboratory analogue materials overemphasizes the damping constant of the lattice vibrations. Furthermore, temperature effects have to be taken into account.

The width of the band is obviously influenced by the dust temperature (Henning & Mutschke 1997; Bowey et al. 2001; Chihara et al. 2001). The reduction of the band widths due to temperature decrease is more pronounced in the FIR and causes less changes in the 10  $\mu\text{m}$  range. According to Bowey et al. (2001), the band widths at 3.5 K are about 90% of the 295 K width in the range from 9 up to 40  $\mu\text{m}$ . The band width reduces to 31% for the 69  $\mu\text{m}$  feature. That means that the combination of temperature and shape effects cannot explain the narrowness of the observed features, especially in the wavelength range up to 40  $\mu\text{m}$ . In the FIR range, the narrowing seems to be more pronounced. According to Chihara et al. (2001), the  $FWHM$  of the 49.8  $\mu\text{m}$  decreases from 0.59 to 0.17  $\mu\text{m}$

**Table 2.** Characteristics of selected forsterite features. Minimum and maximum  $FWHM$  of features observed in circumstellar dust shells from Molster (2000) are compared to  $FWHM$  from calculations of spheres and ellipsoids and CDE1. All data are given in  $\mu\text{m}$ .

feature	observed	sphere/ell.	CDE1
$\lambda_{\text{Peak}}$	( $FWHM$ )	( $FWHM$ )	( $FWHM$ )
9.80	0.14... 0.29	0.08	0.49
10.70	0.11... 0.66	0.06	-
11.40	0.38... 0.86	0.06	1.00
16.20	0.08... 0.62	0.36	0.95
33.6	0.52... 1.15	0.65	2.20
36.50	0.25... 0.97	0.63	0.65
69.0	0.46... 1.04	2.30	2.35

at liquid-helium temperature. The 69.7  $\mu\text{m}$  band  $FWHM$  decreases from 1.34 to 0.27. Therefore, the small  $FWHM$ s of observed bands can be caused by temperature effects. However, we should note that the temperature of the crystalline forsterite in circumstellar shells is closer to 100 K than to liquid-helium temperature (Molster 2000).

## 5. Conclusions

We were able to derive optical constants of crystalline Mg-rich olivine and fayalite by reflection spectroscopy. In the case of forsterite we could extend the data by Servoin & Piriou (1973) by two FIR features. These optical constants were used to calculate mass absorption coefficients for wavelengths between 8 and 100  $\mu\text{m}$  for a variety of particle shapes. These data can be used for a direct comparison with ISO SWS data of circumstellar dust shells compiled by Molster (2000). The consideration of different shapes is motivated by condensation experiments (Tsuchiyama 1998) which demonstrate that forsterite forms crystalline euhedral flakes elongated along the  $c$ -axis, when condensing from the gas phase at high temperature. For this reason, we calculated mass absorption coefficients for spheres, ellipsoids elongated along the  $c$ -axis, and distributions of ellipsoids.

An important result of our study is the fact that shape effects play an important role for the interpretation of astronomical spectra, at least in the cases of strong crystalline bands. The comparison between the mass absorption coefficients and the astronomical spectra of optically thin envelopes showed that both sphere-like particles and ellipsoids elongated along the  $z$ -axis are necessary to obtain a convincing band assignment.

Broad distributions of ellipsoids turned out to be unsatisfying, since their  $FWHM$  mismatched the observations pointing to a condensation of crystalline particles from the gas phase where the crystal structure influences the particle shapes.

*Acknowledgements.* This work was supported by the *Deutsche Forschungsgemeinschaft*, DFG project number Do 575/4-1. We thank W. Assmus from the Physical Institute of the University of Frankfurt/Main for supplying the fayalite crystals. We thank G. Born and W. Teuschel for helping with the preparative work.

## References

- Beintema, D. A. 1998, *A&AS*, 255, 507
- Bohren, C. F., & Huffman, D. R. 1983, *Absorption and Scattering of Light by Small Particles* (Wiley, New York)
- Bowey, J. E., Lee, C., Tucker, C., et al. 2001, *MNRAS*, 325, 886
- Bradley, J. P. 1995, *Meteoritics*, 30, 5, 491
- Bradley, J. P., Keller, L. P., Flynn, G. J., et al. 2000, in *Thermal Emission Spectroscopy*, ed. M. L. Sitko, A. L. Sprague, & D. K. Lynch, ASP Conf. Ser., 196, 119
- Brucato, J. R., Colangeli, L., Mennella, V., et al. 1999, *A&A*, 348, 1012
- Cesarsky, D., Jones, A. P., Lequeux, J., et al. 2000, *A&A*, 358, 708
- Chiar, J. E., Tielens, A. G. G. M., Whittet, D. C. B., et al. 2000, *ApJ*, 537, 749
- Chihara, H., Koike, C., & Tsuchiyama, A. 2001, *PASJ*, 53, 243
- Cohen, M., Barlow, M. J., Sylvester, R. J., et al. 1999, *ApJ*, 513, L135
- Cox, P., & Roelfsema, P. R. 1999, in *Solid Interstellar Matter: The ISO Revolution*, ed. L. d'Hendecourt, C. Joblin, & A. Jones (EDP Sciences & Springer, Berlin), 151
- Crovisier, J., Leech, K., Bockelee-Morvan, D., et al. 1997, *Science*, 275, 1904
- Dartois, E., Cox, P., Roelfsema, P. R., et al. 1998, *A&A*, 338, L21
- Day, K. L. 1976, *ApJ*, 203, L99
- Demyk, K., Jones, A. P., Dartois, E., et al. 1999, *A&A*, 349, 267
- Fabian, D., Jäger, C., Henning, Th., et al. 2000, *A&A*, 364, 282
- Gail, H. P., & Sedlmayr, E. 1998, in *The Molecular Astrophysics of Stars and Galaxies*, ed. T. W. Hartquist, & D. A. Williams (Clarendon Press, Oxford), 285
- Hallenbeck, S. L., Nuth, J. A., & Daukantas, P. L. 1998, *Icarus*, 131, 198
- Hanner, M. S. 1999, *Space Sci. Rev.*, 90, 99
- Henning, Th., & Mutschke, H. 2000, in *Thermal Emission Spectroscopy*, ed. M. L. Sitko, A. L. Sprague, & D. K. Lynch, ASP Conf. Ser., 196, 253
- Henning, Th., & Mutschke, H. 1997, *A&A*, 327, 743
- Hofmeister, A. M. 1987, *Phys. Chem. Minerals*, 14, 499
- Hofmeister, A. M. 1997, *Phys. Chem. Minerals*, 24, 535
- Iishi, K. 1978, *Amer. Mineral.*, 63, 1198
- Jäger, C., Mutschke, H., Begemann, B., et al. 1994, *A&A*, 292, 641
- Jäger, C., Molster, F. J., Dorschner, J., et al. 1998, *A&A*, 339, 904
- Jäger, C., et al. 2001, in preparation
- Jones, A. P., Tielens, A. G. G. M., Hollenbach, D. J., et al. 1994, *ApJ*, 433, 797
- Lingenberg, D. 1986, Ph.D. Thesis, University of Frankfurt/M
- Lim, T. L., Molster, F. J., Sylvester, R. J., et al. 2001, *A&A*, 372, 165
- Malfait, K., Waelkens, C., Waters, L. B. F. M., et al., 1998, *A&A*, 332, L25
- Malfait, K., Waelkens, C., Bouman, J., et al. 1999, *A&A*, 345, 181
- Meeus, G., Waters, L. B. F. M., Bouwman, J., et al. 2001, *A&A*, 365, 476
- Molster, F. J., Waters, L. B. F. M., Trams, N., et al. 1999, *A&A*, 350, 163
- Molster, F. J. 2000, Ph.D. Thesis, University of Amsterdam
- Nuth, J. A. 1996, in *The Cosmic Dust Connection*, ed. J. M. Greenberg (Dordrecht, Kluwer), 205
- Ochler, O., & Günthard, H. H. 1969, *J. Chem. Phys.*, 51, 4719
- Papoular, R., Cauchetier, M., Begin, S., & Lecaer, G. 1998, *A&A*, 329, 1035
- Roesler, H. 1981, *Lehrbuch der Mineralogie*, Deutscher Verlag fuer Grundstoffindustrie, Leipzig
- Sandford, S., & Walker, R. M. 1985, *ApJ*, 291, 838
- Sott, A., & Duley, W. W. 1996, *ApJS*, 105, 401
- Servoin, J. L., & Piriou, B. 1973, *Phys. Stat. Sol. (b)*, 55, 677
- Speck, A. K., Hofmeister, A. M., & Barlow, M. J. 2000, in *Thermal Emission Spectroscopy*, ed. M. L. Sitko, A. L. Sprague, & D. K. Lynch, ASP Conf. Ser. 196, 281
- Steyer, T. R. 1974, Ph.D. Thesis, University of Arizona
- Tsuchiyama, A. 1998, *Mineral. J.*, 20, 59
- Waelkens, C., Waters, L. B. F. M., de Graauw, M. S., et al. 1996, *A&A*, 315, L245
- Waelkens, C., Malfait, K., Waters, L. B. F. M., et al. 2000, *tesa.conf*, 53W
- Waters, L. B. F. M., Molster, F. J., de Jong, et al. 1996, *A&A*, 315, L361
- Waters, L. B. F. M., Molster, F. J., Waelkens, C., et al. 1999, in *Solid Interstellar Matter: The ISO Revolution*, ed. L. d'Hendecourt, C. Joblin, & A. Jones (EDP Sciences & Springer, Berlin), 219
- Weisberg, M. K., Zolensky, M. E., & Prinz, M. 1997, *Meteor. Planet. Sci.*, 32, 791
- Wooden, D. H., Harker, D. E., Woodward, C. E., et al. 1999, *ApJ*, 517, 1034
- Zubko, V. G., Mennella, V., Colangeli, L., & Bussoletti, E. 1996, *MNRAS*, 282, 1321